The influence of the Ti⁴⁺ location on the formation of self-assembled nanocomposite systems based on TiO₂ and Mg/Al-LDHs with photocatalytic properties

E.M. Seftel [a,*], M. Mertens [b], P. Cool [a]

[a] *Laboratory of Adsorption and Catalysis, Department of Chemistry, University of Antwerpen (CDE), Universiteitsplein 1, 2610 Wilrijk, Antwerpen, Belgium*
[b] *VITO Flemish Institute for Technological Research, Boeretang 200, B-2400, Belgium*

ARTICLE INFO

ABSTRACT

Herein, we report the formation of TiO₂/LDH self-assembled nanocomposite systems using the *memory effect* property of the layered clay-type materials. Two different synthesis approaches, based on the modification of the initial brucite-like sheets composition, were used in order to investigate the influence of the Ti⁴⁺ location on the quality of the final products: the reconstruction of a calcined MgAl-LDH in a TiOSO₄·xH₂O aqueous solution and the reconstruction of a calcined MgAlTi-LDH in aqueous solution. The reconstruction process, monitored using X-ray diffraction, IR spectroscopy, UV–vis diffuse reflectance spectroscopy, SEM and thermal analysis, produced different structural changes strongly related with the brucite-like sheets composition. The photocatalytic activity of the obtained nanocomposite systems was evaluated for the degradation of the methyl-orange (MO) dye. An intimate contact has been created between the anatase and the brucite-like sheets in the nanocomposite systems, which had a direct influence on the HO• radical production enhancing thus the photocatalytic performances. When comparing the as-synthesized catalysts, the MgAlTi-LDH solid manifests very powerful photocatalytic effect due to the segregation of small, well defined TiO₂ nanoparticles on the highly hydroxilated layered surface. Up to 93% of the dye could be removed by a TiO₂/LDH-type nanocomposite system. Controlled thermal treatment of photocatalytic systems allowed us to tailor the quality of the photocatalytic active sites deposited on the layered support. The use of the TiO₂/LDHs nanocomposites showed multiple advantages highlighted by the increased activity per mass, higher efficiencies at a decreased solid/liquid ratio, decreased reaction times, reduced agglomeration and easy to separate at the end of the processes.

© 2013 Elsevier B.V. All rights reserved.

1. Introduction

Dyes are widely used in industries such as textile, cosmetics, leather or food. However, many organic dyes are toxic to microorganisms and harmful to human being, therefore the removal of dyes is of great interest and importance [1–3]. With the increase of the discharge of industrial effluents many efforts were made toward the development of new technologies for the clean-up of wastewater. In this regard, heterogeneous photocatalysis has proved to be one of the most potential pollution remediation technologies in recent decades [4–7]. Among many candidates for photocatalysts, TiO₂ is one of the most widely used benchmark standard photocatalysts in the field of environmental applications at present and also probably in the future. This semiconductor photocatalyst generates electrons and hole pairs (e⁻/h⁺) upon irradiation with light energy that can be utilized in initiating oxidation and reduction reactions,

respectively. Nevertheless, the recombination of holes and electrons or agglomeration of the fine nanoparticles which may lead to a decreased photocatalytic activity are, among others, current issues to be improved for practical applications [8,9]. Therefore, it is especially interesting to support TiO₂ nanoparticles on suitable substrates for wastewater and atmospheric remediation.

Previously we reported that the use of TiO₂ nanoparticles in the form of nanocomposite with a solid clay-type support may bring several advantages compared to the use of pure TiO₂ powder [8]. These nanocomposites are formed by the combination of TiO₂ nanoparticles with layered double hydroxides (LDHs) solids.

LDHs, also known as hydrotalcite-like materials or anionic clays, are natural or synthetic mixed metal hydroxides relatively simple and cheap to prepare on both laboratory and industrial scales. Layered double hydroxides are described by the general formula $[M_{1-x}^{II}M_x^{III}(OH)_2]^{x+} A_{x/n}^{n-} \cdot m H_2O$, where M^{II} and M^{III} are the divalent and trivalent cations forming the brucite-like sheets and A^{n-} are the anions which are located within the interlayer gallery together with the water molecules. The most representative mineral within LDHs series is Mg₆Al₂(OH)₁₆CO₃·4H₂O hydrotalcite.

Reconstruction of Mg$_3$Al-LDO in aqueous Ti^{4+} solution:

$$\text{Mg}_3\text{Al-LDH} \xrightarrow{\text{500°C}} \text{Mg}_3\text{Al-LDO} \xrightarrow{\text{0,01M TiOSO}_4x\text{H}_2\text{O}} \text{TiO}_2/\text{Mg}_3\text{Al-LDH}$$

Reconstruction of Mg$_3$Al$_{0.5}$Ti$_{0.5}$-LDO in water:

$$\text{Mg}_3\text{Al}_{0.5}\text{Ti}_{0.5}\text{-LDH} \xrightarrow{\text{300-500°C}} \text{Mg}_3\text{Al}_{0.5}\text{Ti}_{0.5}\text{-LDO} \xrightarrow{\text{H}_2\text{O}} \text{TiO}_2/\text{MgAlTi-LDH}$$
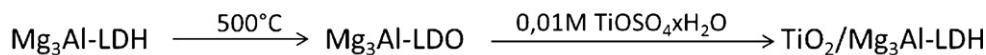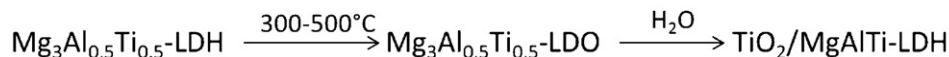
Fig. 1. Schematic representation of the experimental routes followed to obtain the nanocomposite systems.

Their characteristics such as: wide chemical compositions due to variable isomorphic substitutions of metallic cations, variable layers charge density, *memory effect* property, makes them an important "intelligent" family of porous materials [10]. Their thermal stability is strongly related to several factors such as the nature of the cations and the cationic ratio in the brucite-like sheets, the nature of the compensating anions and the crystallinity degree of the LDH lattice [11–13]. Calcination of LDHs solids at moderate temperatures leads to the formation of mixed metal oxides (MMO). The *memory effect* property allows them to rebuild their original layered structure when being in contact with aqueous solutions. Recently it was reported that during the reconstruction process LDHs are also able to adsorb cations from the solution leading to nanostructured assemblies of nanoparticles of metal or metal oxides deposited on the anionic clay matrix [14].

In this study we report the synthesis of some self-assembled nanocomposite systems with unique structure in which LDHs crystallites are embedded into a TiO$_2$ (anatase) matrix. The effect of the brucite-like sheets composition on the formation mechanism of the nanocomposites will be thoroughly investigated. The study will focus on the formation of a TiO$_2$/LDH self-assembled nanocomposite system by two different approaches: (i) structural reconstruction of the calcined MgAl-clay into a TiOSO$_4$ aqueous solution and (ii) structural reconstruction of a calcined MgAlTi-clay in water. In both cases, the growth and organization of the TiO$_2$ nanoparticles on the layered matrix are performed in a single step. Therefore, the influence of the stage where the Ti^{4+} source is added on the formation mechanism will be investigated. Moreover, the ability of the nanocomposites to degrade methyl-orange under UV light will be tested and compared with commercial Degussa P25 TiO$_2$.

2. Experimental details

Two different approaches were applied to obtain the self-assembled nanocomposite systems using the *memory effect* property of the LDHs-type materials (Fig. 1).

2.1. Nanocomposite synthesis

The nitrate form of Mg-Al-layered double hydroxide with the cationic ratios Mg^{2+}/Al^{3+} of 3/1 was synthesized by a simplified co-precipitation and crystallization at 60 °C in the presence of ammonium hydroxide [8]. The obtained product was labeled Mg$_3$Al-LDH. In order to obtain the layered double oxide (Mg$_3$Al-LDO) the obtained Mg$_3$Al-LDH sample was calcined at 500 °C in a Lenton furnace for 6 h (1 °C/min).

2.2. Reconstruction of Mg$_3$Al-LDO in aqueous Ti^{4+} solution

The final TiO$_2$/Mg$_3$Al-LDH nanocomposite system was obtained by max. 1 h contact of Mg$_3$Al-LDO with a 0.01 M solution of TiOSO$_4\cdot x$H$_2$O under vigorous stirring by a modified method which was first described by Carja et al. [14–16]. The aqueous solution of TiOSO$_4\cdot x$H$_2$O contains Ti^{4+} and SO$_4^{2-}$ ions. The Ti^{4+} cations were used to form the TiO$_2$ nanoparticles on the surface of the brucite-like layers and the SO$_4^{2-}$ were used as anionic source during the structural reconstruction process of the parent LDH material. The reaction was realized in N$_2$ atmosphere and the temperature was maintained at 0 °C with an ice cooled water bath. The obtained sample was filtered, washed with distilled water and dried at room temperature. The obtained product was labeled TiO$_2$/Mg$_3$Al-LDH-*t*, where *t* stands for the contact time between the LDO and the aqueous Ti^{4+} solution.

2.3. Reconstruction of Mg$_3$Al$_{0.5}$Ti$_{0.5}$-LDO in water

The nitrate form of Mg-Al-Ti-layered double hydroxide with the cationic ratios Mg^{2+}/Al^{3+}/Ti^{4+} of 3/0.5/0.5 was synthesized using the same simplified co-precipitation and crystallization at 60 °C in the presence of ammonium hydroxide [8]. The obtained product was labeled Mg$_3$Al$_{0.5}$Ti$_{0.5}$-LDH. In order to obtain the layered double oxide (Mg$_3$Al$_{0.5}$Ti$_{0.5}$-LDO) the obtained Mg$_3$Al$_{0.5}$Ti$_{0.5}$-LDH sample was calcined, depending on their thermal stability, at different temperatures in a Lenton furnace for 6 h (1 °C/min).

The TiO$_2$/MgAlTi-LDH nanocomposite systems were obtained by adding the Mg$_3$Al$_{0.5}$Ti$_{0.5}$-LDO into distilled water while stirring at room temperature for 3 h.

The samples were labeled Mg$_3$Al$_{0.5}$Ti$_{0.5}$-T°C-R$_{H2O}$, where T°C stands for the calcination temperature of 300 °C or 500 °C, respectively.

2.4. Photocatalytic experiments

The photocatalytic activities of all samples were tested for the photodegradation of methyl orange in aqueous solution. An appropriate amount of a catalyst was dispersed into a methyl orange (MO) solution (4×10^{-5} M) in a plastic flask and stirred for 30 min. prior to UV irradiation in order to establish the adsorption–desorption equilibrium between the dye and the catalyst surface. Next, the suspension was irradiated with UV-light for 60 min. The UV-light source was a 100 W Hg lamp (Sylvania Par 38, 365 nm). The concentration of methyl orange dye in aqueous solution was monitored by measuring the light absorption at 463 nm of the specimens taken from the reaction system with a Thermo-electron evolution 500 UV–vis Spectrometer using water as reference.

2.5. Characterization techniques

The chemical composition of the final products was determined by electron probe micro analysis measurements (EPMA).

The structure and the crystal phases of the as synthesized solids were investigated by X-ray diffraction (XRD), FT-IR and UV–vis

diffuse reflectance spectroscopy (UV–vis-DR), TG/DTA, N_2 adsorption/desorption and scanning electron microscopy methods.

X-ray diffractions were recorded on a PANalytical X'Pert PRO MPD diffractometer with filtered CuKα radiation; measurements were done in the 2θ mode using a bracket sample holder with a scanning speed of 0.04°/4 s in continuous mode. Diffuse reflectance infrared Fourier transform spectra (DRIFT) were measured on a Nicolet 20 DXB FTIR Spectrometer, equipped with a spectra-tech diffuse reflectance accessory. About 200 scans were taken with a 4 cm^{-1} resolution. UV–vis-DR spectra were obtained at room temperature on a NICOLET EVOLUTION 500 UV–vis Spectrometer, with a diffuse reflectance accessory using KBr standard white as reflectance.

TG/SDTA technique was used to obtain information about the thermal stability of the samples and possible phase transformations. The measurements were performed on a Mettler TGA/SDTA851^e SF/1100 °C thermo-balance, equipped with a MT1 microbalance. Samples were heated in an alumina crucible (70 μl capacity) at a heating rate of 5 °C/min under O_2 or N_2 atmosphere (flow rate of 30 cm^3/min) up to 1000 °C. DTA figures presented here were weight-normalized (1 min^{-1} vs. °C). Corrections were made by measuring empty alumina crucibles under identical conditions as the samples to exclude buoyancy effects. The results shown here were then obtained by subtracting the blank from the sample.

The surface area and porosity of the prepared materials were determined via N_2-sorption on a Quantachrome Quadrasorb SI automated gas adsorption system. The Mg$_3$Al-LDH and TiO$_2$/Mg$_3$Al-LDH samples were outgassed at room temperature to prevent structural changes upon degassing. All the other calcined samples were outgassed at 200 °C for 16 h. After degassing, N_2-sorption was carried out at −196 °C. The Brunauer–Emmet–Teller (BET) method was applied to calculate the specific surface area. The volume adsorbed at a relative pressure $P/P_0 = 0.98$ was applied to determine the total pore volume.

The SEM images were obtained using a JSM 5510 microscope, operating at an accelerating voltage of 15 kV.

3. Results and discussions

3.1. Composition and structure of the reconstructed nanocomposites

In order to study the influence of the initial Ti^{4+} location on the quality of the final products, two different approaches were used to obtain the nanocomposites by taking advantage of the *memory effect* property of the layered double hydroxide materials: the reconstruction of a MgAl-layered double oxide (LDO) in a TiOSO$_4 \cdot x$H$_2$O aqueous solution and the reconstruction of a MgAlTi-LDO in aqueous solution (Fig. 1).

The first approach is based on the hypothesis that the calcined LDHs are able not only to take anions from an aqueous solution to rebuild their interlayers but also to adsorb cations from the solution [14]. Therefore, the titanium precursor containing the sulphate anions have a double role: as anionic source in the reconstruction of the interlayer and secondly, to provide the Ti^{4+} cations for the formation of the TiO$_2$ nanoparticles on the surface of the brucite-like layers by a self-assembly mechanism realized in a single and fast synthetic step.

The second approach involves the use of an LDH-type material which contains the Ti^{4+} cations inside the brucite-like sheets. Therefore, the brucite-like sheets composition was altered before the reconstruction step. These two modifications of the reconstruction process may lead to TiO$_2$/LDHs nanocomposites in which the contact between the two components may be different, thus affecting the photocatalytic performances of the final materials.

Table 1
Structural characteristics for the studied samples obtained by the first synthesis approach.

	Mg$_3$Al-LDH	TiO$_2$/Mg$_3$Al-LDH-1 h
a (Å)	3.04	3.051
c (Å)	25.74	23.55
c' (Å)	8.58	7.85
[a]The thickness of the interlayer gallery (Å)	3.78	3.05
XRD phase observed	LDH	LDH + anatase
[b]wt% Ti^{4+} (TiO$_2$ respectively)	–	13.7 (22.9)
[c]Identified anion	NO$_3$$^-$	SO$_4$$^{2-}$
[d]LDH crystallite size in c direction (D_{003}) (nm)	5.09	4.08

$a = 2d_{110}$, $c = 3d_{003}$ and $c = 3c'$.

[a] The difference between c' and 4.8 Å (the thickness of the brucite-like sheet) [10].
[b] Calculated from the EPMA results.
[c] Based on the interlayer thickness value and FTIR observations;
[d] Calculated using the Scherrer equation [19].

3.1.1. Structural characterization of the TiO$_2$/Mg$_3$Al-LDH nanocomposites

Fig. 2 displays the XRD patterns of the as-synthesized and reconstructed layered double hydroxides. The X-ray diffraction pattern of the parent Mg$_3$Al-LDH sample displays the characteristic symmetric and sharp peaks due to the basal planes (0 0 3) and (0 0 6) together with asymmetric reflections, less sharp due to the (1 0 1), (0 1 5) and (0 1 8) and (1 1 0) planes which are normally observed for LDH with rhombohedral structures containing NO$_3$$^-$ as interlayer anion [8,17].

Several differences may be observed after the reconstruction step in the XRD pattern of the obtained nanocomposite sample (Fig. 2b). First, the basal spacing is decreasing from 8.58 Å to 7.85 Å indicating the replacement of the nitrate anions with the sulphate anions in the interlayer gallery (Table 1) [18]. Secondly, some new extra peaks are observed at 36.5° and 38.3° 2θ degrees which may be associated with the formation of very small titania crystallites in anatase form. Furthermore, the unit cell parameter a is also observed to be slightly increased when the layered structure was reconstructed in titanium oxysulphate aqueous solution (Table 1). This observation may be explained taking into account the ionic radii of the metal cations (0.65 Å for Mg^{2+}, 0.5 Å for Al^{3+} and 0.61 Å for Ti^{4+}) as well as the metal-oxygen bond lengths (2.11 Å for Mg-O, 1.90 Å for Al-O and 1.95 Å for Ti-O) [10,12,19]. The a unit cell parameter of LDHs corresponds to the cation-cation distance within the brucite-like layer and can be calculated by $a = 2 \times d(1 1 0)$. Therefore, it can be concluded that during the reconstruction process part of the Ti^{4+} cations are incorporated in the brucite-like sheets. In addition, a decrease in crystallinity may be observed for the reconstructed sample in comparison to the parent LDH sample. These two last observations may be due to the reconstruction process which is based on a dissolution-recrystallization mechanism, leading to the partial incorporation of the Ti^{4+} in the layered structure. Moreover, the decrease in crystallinity may also be assigned to the partial incorporation of the Ti^{4+} cations in the brucite-like sheets. Since only two small reflections correlated with the titania crystallites were identified in the XRD profile and taking into account all above observations, it can be concluded that only small part of the titanium exists as an TiO$_2$ anatase phase, the rest of the Ti^{4+} cations being incorporated in the brucite-like sheets.

However, the XRD pattern is sufficiently well resolved in order to distinguish between the combination of the two phases, i.e. the titania and the layered structure, and there is no doubt that the structural memory effect has been triggered.

The FTIR Spectroscopy technique has been used to identify the nature of the anionic species in the interlayer gallery before and
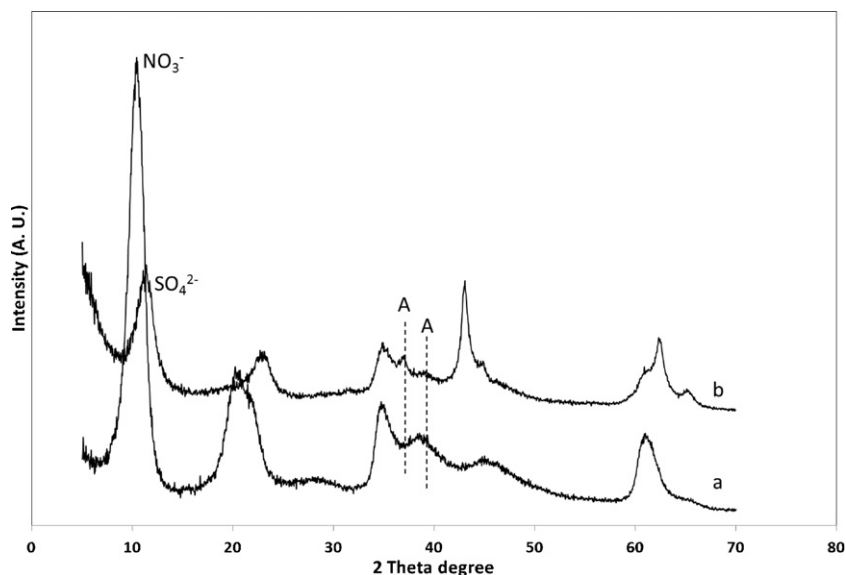
Fig. 2. The XRD patterns of (a) Mg$_3$Al-LDH and (b) TiO$_2$/Mg$_3$Al-LDH-1 h samples. A – anatase phase.

after the self-assembly process. Fig. 3 shows the FTIR spectra of the as-synthesized and reconstructed LDH-type material.

The as-synthesized Mg$_3$Al-LDH sample shows a broad and intense band between 3600 and 3300 cm^{-1} centered at ~3500 cm^{-1} which may be attributed to the stretching vibration of the OH groups in the brucite-like layers and the interlamellar water molecules. The nitrate anions are identified in the interlayer gallery of the as-synthesized material by the presence of the infrared band at 1375 cm^{-1} which may be assigned to the ν_3 stretching vibration of the NO$_3^-$ groups. The appearance of the vibration bands at ~820 cm^{-1} and ~1740 cm^{-1} are attributed to the stretching modes and confirm the presence of the NO$_3^-$ groups in the interlayer gallery of the LDH precursor with the D_{3h} symmetry. Differences appear in the FTIR spectra after the structure is reconstructed in a titanium oxysulphate solution. The presence of the sulphate anions may be observed by the appearance of the specific bands at ~1120 cm^{-1} and 660 cm^{-1} which may be assigned to the ν_3 and ν_4 vibrations modes of SO$_4^{2-}$ in the interlayer space of the reconstructed sample. Major difference

may be observed in the high frequency region of the FTIR spectra. This band is now splitted into two bands, at ~3500 cm^{-1} and ~3100 cm^{-1} indicating the combination of the LDH [19,20] with the titania phase [21], respectively.

The thermal stability of the obtained self-assembled nanocomposite was studied using the TG/SDTA technique. Representative SDTA and TGA curves of the nanocomposite sample are shown in Fig. 4.

Three weight losses may be observed in the TGA profile at temperatures of ca. 30–230 °C, 230–450 °C and 937 °C and above. All these steps are endothermic. The first weight loss may be associated with the removal of adsorbed and intercalated water molecules [11]. The second one, at higher temperatures is due to the dehydroxylation of the brucite-like sheets and is associated with the structural collapse of the LDH phase during heating [11,22]. The last weight loss involves the beginning of the SO$_4^{2-}$ loss as sulfur dioxide [22]. The upper limit of the TG experiment is 1000 °C and some sulphate is retained until higher temperatures. Therefore, the mass loss cannot be clearly observed from the thermogravimetric
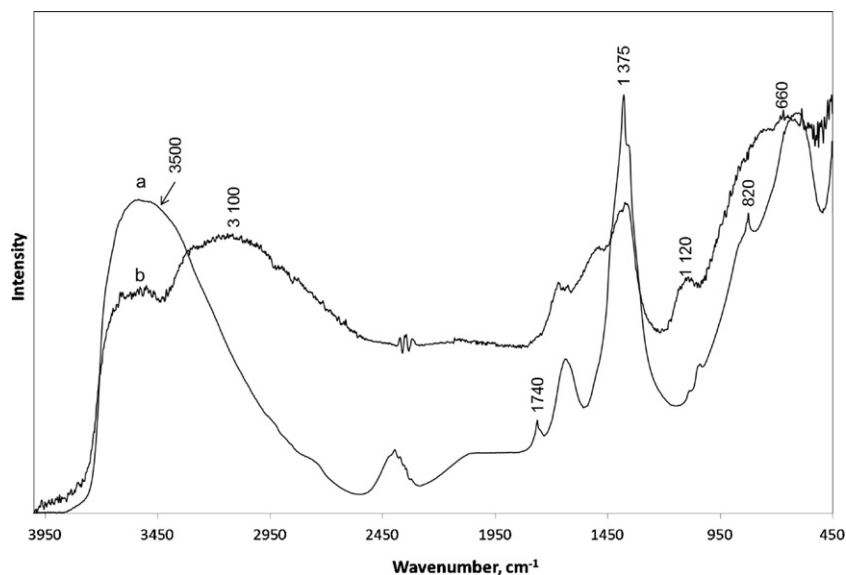

Fig. 3. The FTIR spectra of (a) Mg$_3$Al-LDH and (b) TiO$_2$/Mg$_3$Al-LDH-1 h samples.

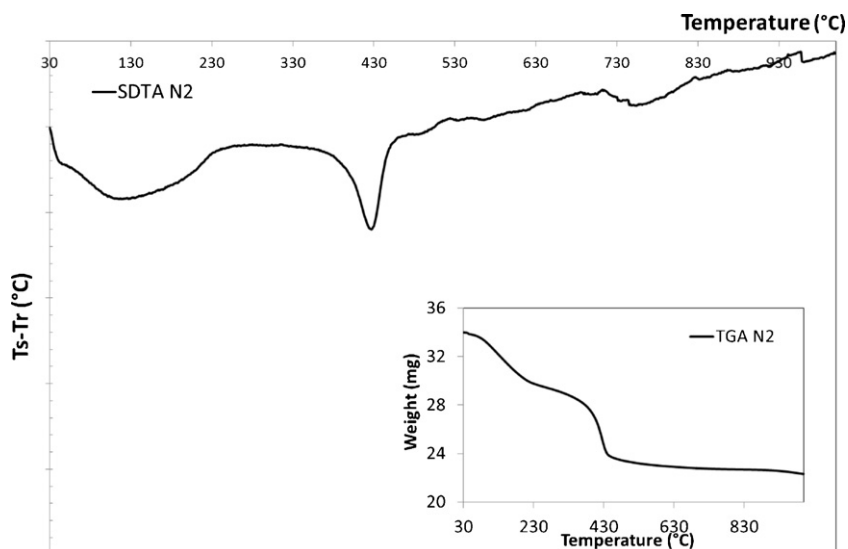**Fig. 4.** Thermoanalytical curves (SDTA/TGA) of the TiO_2/Mg_3Al-LDH-1 h sample.

curve. Additionally, an extra endothermic transition is observed at ca. 650–750 °C in the SDTA curve, with no concomitant mass loss in the TGA profile. Taking into account the XRD observations of the as-synthesized nanocomposites and correlating with the XRD analysis of the calcined products (see Fig. 5), this step may be associated with the complete crystallization and growth of the TiO_2 nanocrystals in the nanocomposite system.

Accordingly, it can be observed that after the thermal treatment at 450 °C (Fig. 5b), the structural collapse of the layered phase occurs together with the growth of the already formed anatase crystals as indicated by the disappearance of the reflection at 11.06° (2θ) and the increase of the intensity of the peak centered at 36.86 (2θ), respectively. After the calcination at 750 °C (Fig. 5c) the complete crystallization and growth of the TiO_2 is observed, as indicated by the presence of the peaks at $2\theta = 25.5°$, 36.82°, 48.0°, 53.8°, 54.9°, 68.62° and 70.14° corresponding to the reflections from (1 0 1), (1 0 3), (2 0 0), (1 0 5), (2 1 1), (1 1 6) and (2 2 0) planes characteristic for the anatase crystalline phase [8].

Evidence of the preservation of small amounts of layered structure in the calcined materials was obtained using the Infrared Spectroscopy combined with chemical analysis and SEM

observations. Upon reconstruction, the morphology is completely changed even in the presence of very diluted $TiOSO_4 \cdot xH_2O$ solution as indicated by the SEM analysis (Fig. 6). When the calcined form of the Mg_3Al-LDH sample is reconstructed in distilled water, a house-of-cards layered structure typical for the LDH-type materials is observed (Fig. 6A). This morphology completely changes into spherical particles even when very diluted Ti^{4+} aqueous solutions are added in the reconstruction process.

The chemical analysis of the nanocomposites revealed that upon calcination the cationic ratio $Ti^{4+}/(Mg^{2+} + Al^{3+})$ increase. Taking into account the weight and size of these cations, the increase of the cationic ratio may be correlated with the diffusion of the Mg^{2+} and Al^{3+} (which are forming the layered structure) to the core of the particles [23]. Therefore, nanocomposite systems are formed in which the core is Mg and Al enriched (small regions of LDH structure) and the particle surface is constituted by TiO_2 phase. The infrared data are in agreement with this assumption. The IR spectra recorded for the uncalcined and calcined nanocomposites were compared with the one of pure Mg_3Al-LDH (Fig. 7). Usually, the vibration band at 1375 cm^{-1} associated with the nitrate anions disappears when the LDH decomposes [10,11]. In our case, this band is always
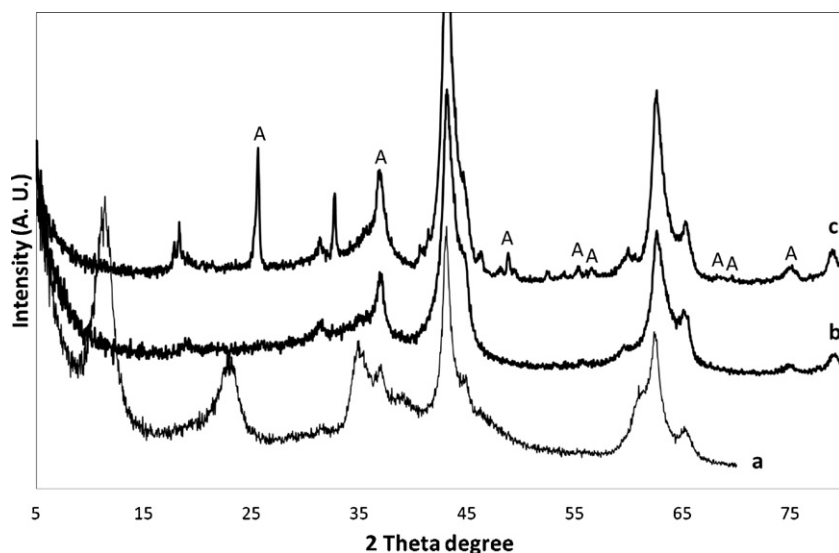

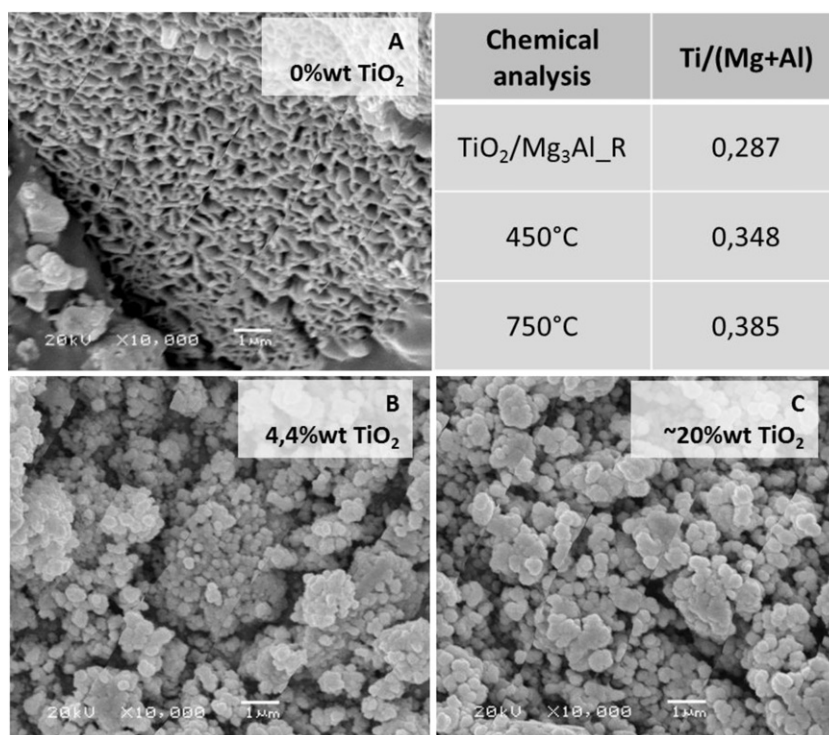**Fig. 5.** The XRD patterns of the (a) TiO_2/Mg_3Al-LDH-1 h nanocomposite and calcined at (b) 450 °C and (c) 750 °C. A – anatase phase.

Fig. 6. SEM micrograph of calcined Mg_3Al-LDH sample (A) reconstructed in water, (B) reconstructed in very diluted $TiOSO_4 \cdot xH_2O$ and (C) reconstructed in 0.01 M $TiOSO_4 \cdot xH_2O$ solution (chemical analysis using EPMA technique).

present indicating that the layered structure is not fully destroyed [24,25].

At first sight, these results are in disagreement with the XRD data obtained for the calcined samples presented in Fig. 5. Moreover, to observe a compound by X-ray diffraction it has to be present in more than 3%, the crystallite size has to be larger than ca. 25 Å and located on the surface [11,23]. In our case, the LDH structure is sheltered with large amounts of TiO_2 phase and could not be detected with X-ray diffraction. In infrared spectroscopy, a band appears below these constrains, therefore it can be concluded that core–shell type nanostructures are formed in which small amounts of LDH phase are encapsulated into a TiO_2 anatase matrix. The

formation of combined anatase-LDH nanocomposite is also demonstrated by the presence of a vibration band which is splitted in the high frequency region in the FTIR spectra (Fig. 7).

3.1.2. Structural characterization of the TiO_2/MgAlTi-LDH nanocomposites

It was previously reported that the attempt to incorporate tetravalent cations within the brucite-like sheets leads to the partial segregation of these cations on the surface of the layered structure [26]. Recently we have investigated the incorporation of Ti^{4+} in a ZnAl-LDH and we have found that approximately 50% of Ti^{4+} could be incorporated within the brucite-like sheets forming the
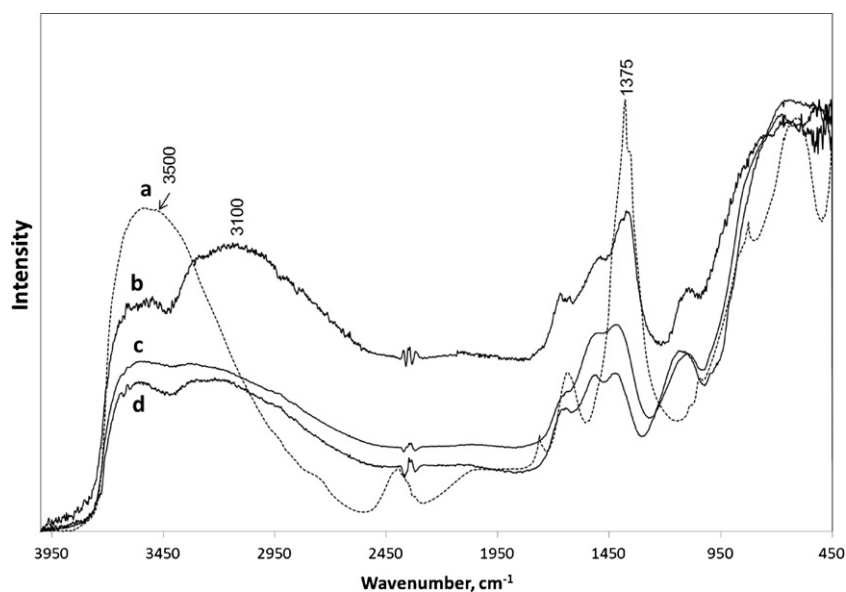

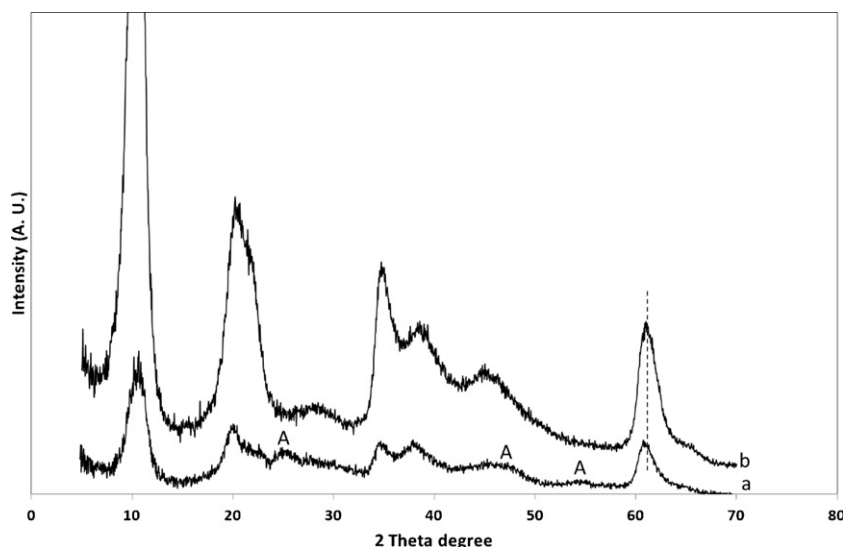**Fig. 7.** The infrared spectra of (a) Mg_3Al-LDH, (b) TiO_2/Mg_3Al-LDH-1 h nanocomposite and calcined at (c) 450 °C and (d) 750 °C.

Fig. 8. The XRD patterns of the (a) $Mg_3Al_{0.5}Ti_{0.5}$-LDH and (b) Mg_3Al-LDH samples. A – anatase phase.

layered structure and the other part segregated as an amorphous TiO_2 phase [19]. Velu et al. reported the possibility of incorporation of Sn^{4+} into LDH-type layers over a large composition range and claimed that up to 30% of Al^{3+} could be substituted by Sn^{4+} to form a new MgAlSn ternary LDH [27].

In the present synthetic conditions, the XRD pattern of the as-synthesized Ti-containing layered product (Fig. 8a) displays the reflections characteristic to the LDH materials [10,28].

In addition to the LDH phase, TiO_2 with anatase crystal structure may be identified from the appearance of some additional peaks centered at 25.01°, 48.0° and 54.38° 2θ degrees. The increase of the a parameter value together with the decreased crystallinity of the obtained layered product may be an indication that the Ti^{4+} cations are partially incorporated in the brucite-like network (Table 2).

Prior to the calcination step, the thermal stability of the as-synthesized $Mg_3Al_{0.5}Ti_{0.5}$-LDH sample was evaluated using the TG/DTG technique. The DTG profiles are displayed in Fig. 9. In comparison with the DTG profile of the Mg_3Al-LDH sample, the Ti-containing sample shows three weight losses. The first weight loss may be associated with the loss of the water molecules from the outer surface as well as from the interlayer gallery, followed by a weight loss at ∼260 °C which may be associated with the dehydroxylation of the Ti–OH groups. The last weight loss observed in the range of 350–500 °C is due to the dehydroxylation of the brucite-like sheets showing that the layered structure decreases its stability when the Ti^{4+} cations are introduced in the brucite-like sheets. These results are in agreement with the XRD observations showing that only part of the Ti^{4+} cations are isomorphously substituted in the brucite-like network, the rest of them forming TiO_2 regions on the LDH surface.

Therefore, the $Mg_3Al_{0.5}Ti_{0.5}$-LDH sample was calcined at 300 °C and 500 °C followed by the reconstruction of the initial structure in aqueous media. Figs. 10 and 11 show the XRD patterns of the calcined, at 300 °C and 500 °C, as well as reconstructed products, respectively.

The XRD pattern of the $Mg_3Al_{0.5}Ti_{0.5}$-300 °C-R_{H2O} is clearly different from the one obtained for the $Mg_3Al_{0.5}Ti_{0.5}$-500 °C-R_{H2O} sample. This difference is originating from the different structures obtained at different thermal treatments. Correlating with the observations obtained from the thermal analysis, when the sample is calcined at 300 °C, the layered structure is still intact. This means that only the dehydroxylation of the TiO_2 phase occurs, with no concomitant diffusion of the Ti^{4+} cations within the brucite-like sheets. This observation is also supported by the a parameter value, which is not modified after the sample is thermally treated at 300 °C. Moreover, the loss of the interlayer water molecules occurs leading to a contraction of the LDH structure in the (0 0 3) direction having as effect the decrease in the c parameter value (Table 2). At this stage of reaction, only the further crystallization and slight growth of the anatase nanoparticles occurs. Therefore, the final product obtained after being in contact with aqueous media is the combination of the layered LDH structure together with small and well crystallized TiO_2 anatase nanoparticles (of ∼6 nm).

At the moment when the sample is calcined at 500 °C, the dehydroxylation of the LDH phase occurs, the calcination product being a layered mixed oxide phase. When the calcination product is placed in contact with the aqueous media, a different reconstruction process occurs. The XRD pattern of the reconstructed $Mg_3Al_{0.5}Ti_{0.5}$-500 °C-R_{H2O} sample (Fig. 11c) shows the formation of the characteristic layered structure which is the predominant phase. Only minor traces of TiO_2 with anatase crystal phase may

Table 2
Structural characteristics for the studied samples obtained by the second synthesis approach.

Sample	a (Å)	c (Å)	XRD phase observed	[a]TiO_2 D_{101} (nm)	[b]LDH D_{003} (nm)
Mg_3Al-LDH	3.04	25.74	LDH	–	5.09
$Mg_3Al_{0.5}Ti_{0.5}$-LDH	3.054	26.04	LDH + anatase	3.43	3.88
$Mg_3Al_{0.5}Ti_{0.5}$-300 °C	3.05	23.55	LDH + anatase	4.02	2.3*
$Mg_3Al_{0.5}Ti_{0.5}$-300 °C-R_{H2O}	3.05	24.78	LDH + anatase	6.03	4.86
$Mg_3Al_{0.5}Ti_{0.5}$-500 °C	–	–	LDO	–	–
$Mg_3Al_{0.5}Ti_{0.5}$-500 °C-R_{H2O}	3.06	23.64	LDH	–	8.09

$a = 2d_{110}$; $c = 3d_{003}$.
[a,b]Calculated using the Scherrer equation [19]. *low intensity XRD reflection – approx. value.
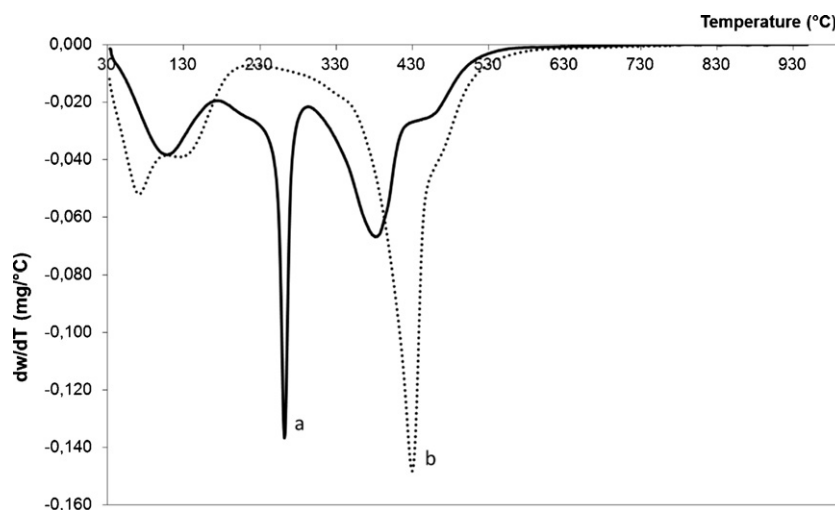
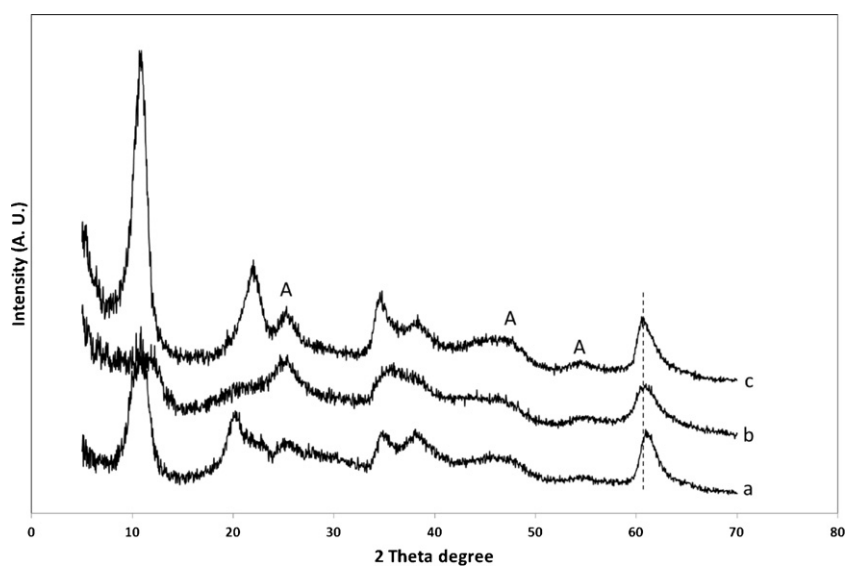**Fig. 9.** The DTG profiles characteristic for the (a) $Mg_3Al_{0.5}Ti_{0.5}$-LDH and (b) Mg_3Al-LDH samples.

Fig. 10. The XRD patterns of the (a) $Mg_3Al_{0.5}Ti_{0.5}$-LDH, (b) $Mg_3Al_{0.5}Ti_{0.5}$-300 °C and (c) $Mg_3Al_{0.5}Ti_{0.5}$-300 °C-R_{H2O}. A – anatase phase.
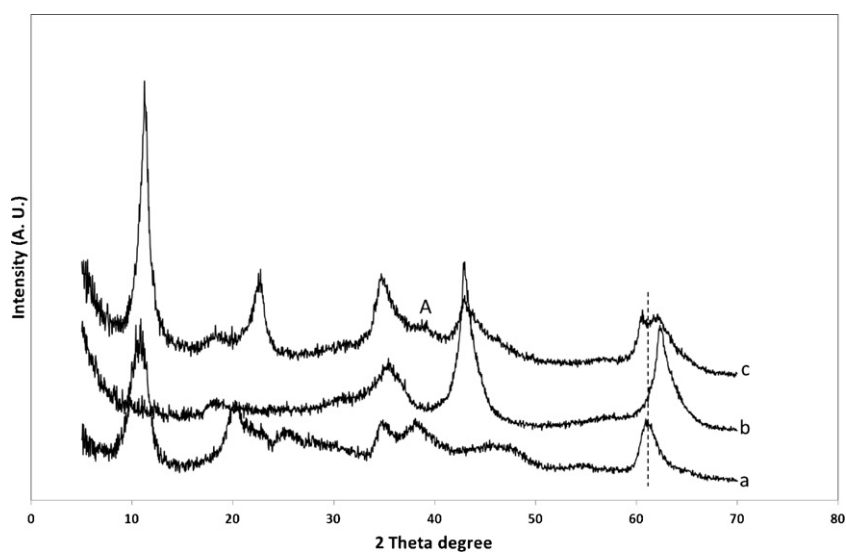
Fig. 11. The XRD patterns of the (a) $Mg_3Al_{0.5}Ti_{0.5}$-LDH, (b) (b) $Mg_3Al_{0.5}Ti_{0.5}$-500 °C and (c) $Mg_3Al_{0.5}Ti_{0.5}$-500 °C-R_{H2O}. A – anatase phase.
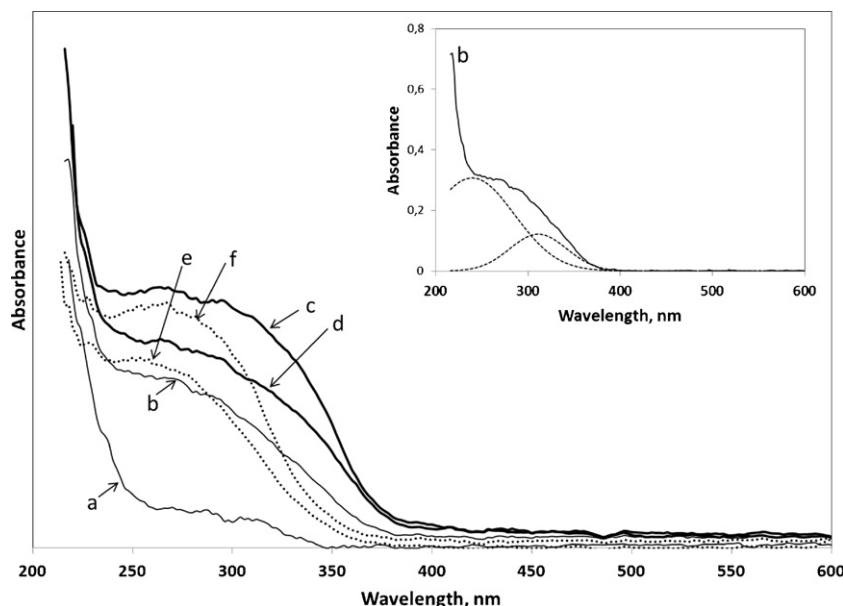
Fig. 12. The DRS spectra of (a) Mg_3Al-LDH, (b) $Mg_3Al_{0.5}Ti_{0.5}$-LDH, (c) $Mg_3Al_{0.5}Ti_{0.5}$-300 °C, (d) $Mg_3Al_{0.5}Ti_{0.5}$-300 °C-R_{H2O}, (e) $Mg_3Al_{0.5}Ti_{0.5}$-500 °C and (f) $Mg_3Al_{0.5}Ti_{0.5}$-500 °C-R_{H2O} samples. The inset picture: band component analysis of the (b) $Mg_3Al_{0.5}Ti_{0.5}$-LDH sample.

be observed by the presence of a very small reflection centered at $2\theta = 38.22°$. Moreover, the value of the a parameter is found to increase from 3.05 Å to 3.06 Å indicating the incorporation of more Ti^{4+} cations within the brucite-like sheets. Therefore, it might be concluded that during the reconstruction process of the sample calcined at 500 °C, the initially segregated Ti^{4+} cations diffuse into the layered network, the final material being almost 100% LDH phase.

The UV–vis Diffuse Reflectance Spectroscopy was used to investigate the environment and the coordination state of the Ti^{4+} cations in the obtained nanocomposites. The DRS spectra of the studied samples are shown in Fig. 12. The parent Mg_3Al-LDH sample exhibits relatively low absorption in the UV–vis DR spectra. At the moment when the Al^{3+} cations are partially substituted by the tetravalent Ti^{4+} cations, a broad absorption is observed in the range of 238–360 nm (Fig. 12b and the inset picture). This broad absorption can be assigned to a combination of two overlapping absorptions. First, an absorption band at lower wavelengths 238–260 nm which can be assigned to the ligand-to-metal charge transfer involving Ti atoms in octahedral coordination [29,30]. The second absorption band between 320 and 360 nm can be attributed to the presence of some Ti atoms in an octahedral environment participating at Ti–O–Ti bonds as part of small TiO_2 regions [19]. These observations are in good agreement with the XRD data (Fig. 8) showing that when the ternary MgAlTi-layered material was synthesized, partial segregation of the Ti^{4+} cations occurred.

The DRS spectra of the $Mg_3Al_{0.5}Ti_{0.5}$-300 °C and $Mg_3Al_{0.5}Ti_{0.5}$-300 °C-R_{H2O} samples show the same trend as the uncalcined layered product indicating the presence of both types of environments for the Ti atoms. When the sample is reconstructed in aqueous media, the DRS profile is more intense and well defined indicating the complete crystallization of anatase nanoparticles on the surface of the brucite-like sheets.

On the contrary, the DRS spectrum obtained for the sample calcined at 500 °C (Fig. 12e) indicates the presence of only one broad absorption centered at ~260 nm indicating that the Ti atoms have octahedral coordination. The same trend is observed after the reconstruction process indicating that all the Ti cations are now located within the brucite-like sheets.

These results are in good agreement with the XRD and DTG observations showing that the thermal treatment at 300 °C does not modify the location of the Ti atoms within the framework obtaining a nanocomposite structure in which an intimate contact has been created between the anatase nanoparticles and the layered structure. On the other hand, the treatment at 500 °C promotes the diffusion of the Ti^{4+} cations inside the brucite-like sheets, the final material being composed only from the LDH phase.

Moreover, the investigation of the morphology using SEM technique supports the above assumptions. Fig. 13 displays the SEM micrographs of the samples obtained at different thermal treatment and exposed at aqueous media to rebuild the layered structure. As it can be observed, the $Mg_3Al_{0.5}Ti_{0.5}$-300 °C-R_{H2O} is
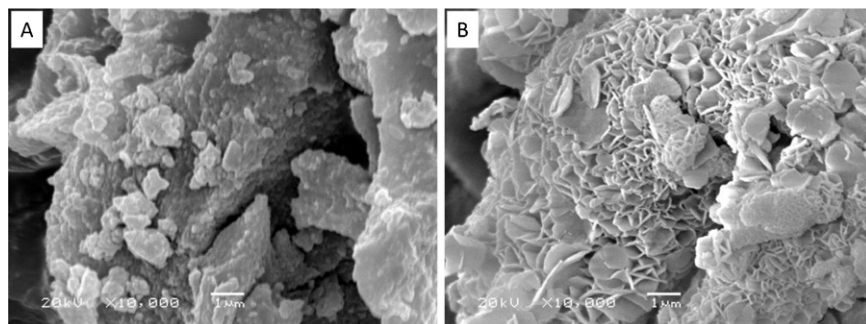
Fig. 13. The SEM micrographs of (A) $Mg_3Al_{0.5}Ti_{0.5}$-300 °C-R_{H2O} and (B) $Mg_3Al_{0.5}Ti_{0.5}$-500 °C-R_{H2O} samples.
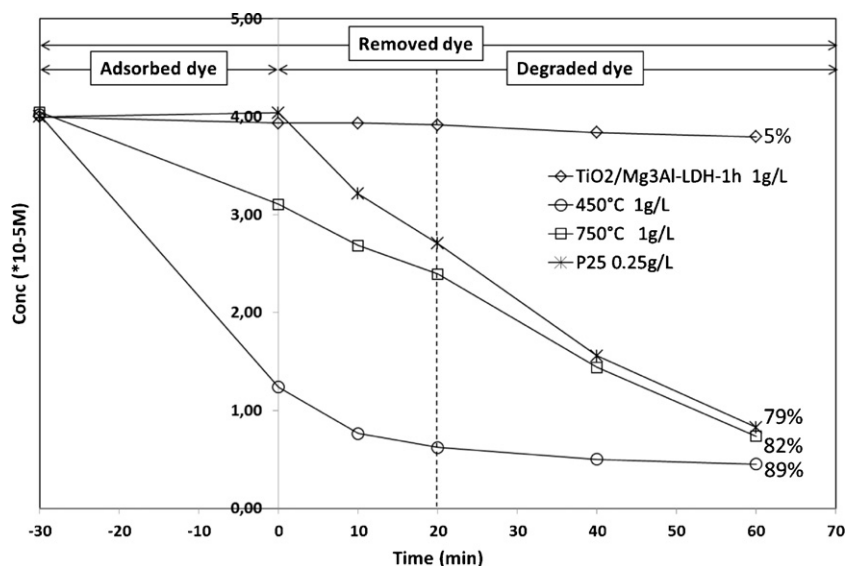
Fig. 14. The kinetic curves of the methyl-orange degradation in the presence of the uncalcined and calcined form of the TiO_2/Mg_3Al-LDH-1 h nanocomposites and compared with commercial Degussa P25.

observed as large and compact chunks with segregated smaller nanoparticles. On the other hand, when the sample is calcined at 500 °C the LDH structure collapses and a solid solution is produced which, placed in aqueous media, promotes the diffusion of the Ti^{4+} cations within the brucite-like sheets obtaining materials with typical interconnected hexagonal platelets. This morphology is in agreement with the above formulated hypotheses indicating the complete incorporation of Ti^{4+} cations and regeneration of layered structure without any segregation of Ti^{4+} cations.

3.2. Photocatalytic evaluation of the obtained nanocomposites

3.2.1. Photocatalytic evaluation of the TiO_2/Mg_3Al-LDH nanocomposites

The catalytic tests were realized at a catalyst dose of 1 g/L. It should be noted that the final composition, analyzed using the EPMA technique, revealed that the TiO_2 phase accounts for ∼1/4 of the total weight of the nanocomposite system. Therefore, the same amount of commercial Degussa P25 (0.25 g/L) was used for a comparative photocatalytic test. Compared with the commercial P25, the nanocomposites demonstrated enhanced photocatalytic activity.

The methyl-orange degradation profiles obtained with TiO_2/Mg_3Al-LDH-1 h nanocomposites are shown in Fig. 14. As expected, the as-synthesized nanocomposite shows very low photocatalytic activity. This result may be well correlated with the XRD observations indicating at this stage of the nanocomposite synthesis, only small amount of titanium exists as an anatase phase, the rest of the Ti^{4+} cations being incorporated in the brucite-like sheets.

Improved photocatalytic activity may be observed after the samples were exposed at controlled thermal treatment. It is interesting to note that the sample calcined at 450 °C follows different reaction path than the sample calcined at 750 °C. More specific, in the case of the sample calcined at 450 °C, 89% of methyl-orange could be removed mainly due to the MO adsorption followed by a gradual decrease of MO concentration due to a photocatalytic reaction. Going further with the thermal treatment up to 750 °C, the observed dye removal percentage (82%) can be assigned mainly to a photocatalytic process. This behavior of the different thermally treated samples may be well correlated with the XRD observations showing that the crystallization of the TiO_2 anatase phase starts at

450 °C and continues up to 750 °C where well-defined and structured anatase crystallites are obtained. Moreover, the calcination of LDHs gives rise not only to changes in their structure, but also to changes in their surface area and pore development [10,11,27]. The increased dye adsorption in the first 30 min by the sample calcined at 450 °C can be associated with the increased surface area (112 m^2/g). When the sample is calcined at 750 °C the porosity was found to decrease to 99 m^2/g which may be associated with the crystallization and growth of the TiO_2 anatase nanoparticles in the inner space of the mesopores. The decrease of the porosity when the sample is calcined at 750 °C is also reflected in the adsorption behavior observed during the photocatalytic tests (Fig. 14). Taking for example the dye concentration after 20 min. of photocatalytic test it can be concluded that the sample calcined at 450 °C is much more effective that the other studied samples or the commercial Degussa P25.

3.2.2. Photocatalytic evaluation of the $TiO_2/MgAlTi$-LDH nanocomposites

Fig. 15 shows the kinetic curves obtained during the photocatalytic tests on the methyl-orange degradation in aqueous media in the presence of the $TiO_2/MgAlTi$-LDH nanocomposites. The catalytic tests were realized at a catalyst dose of 0.5 g/L. The final composition, analyzed using the EPMA technique, revealed that the TiO_2 phase accounts for ∼1/5 from the total weight of the nanocomposite system. Therefore, the same amount of P25 (0.1 g/L) was used for a comparative photocatalytic test. Compared with the commercial P25, the nanocomposites demonstrated enhanced photocatalytic activity.

It can be observed that the as-synthesized $Mg_3Al_{0.5}Ti_{0.5}$-LDH sample manifests already very powerful photocatalytic effect which may be due to the decreased size of the anatase nanoparticles in combination with highly hydroxylated layered surface. It was previously reported that the materials rich in OH groups, like LDHs, may favor the titania activity [31]. The surface hydroxyl groups may be easily converted into HO• radicals, which are the primary species responsible for the dye degradation [31,32]. When the sample is calcined at 300 °C and reconstructed in aqueous media, the final product shows decreased degradation efficiency. This behavior may be explained in terms of increased crystal size of the anatase nanoparticles as well as surface coverage of the layered phase with the TiO_2 phase. In this case, the TiO_2 may block some structural OH
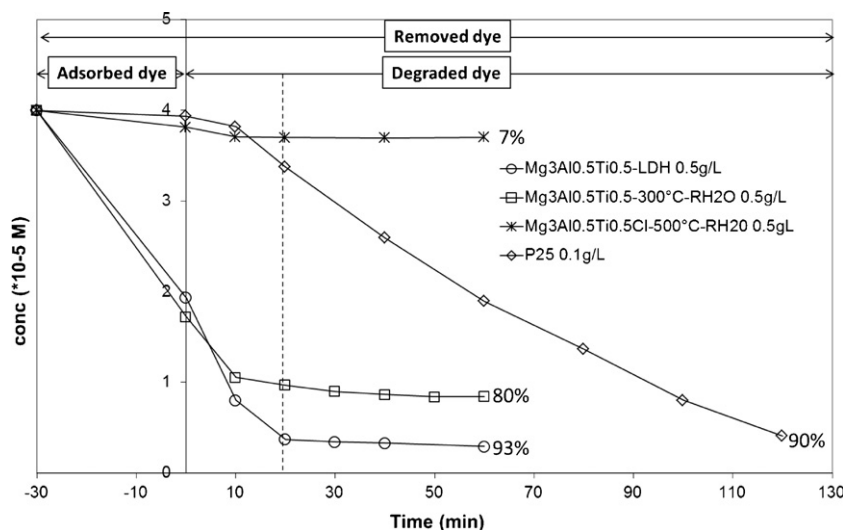
Fig. 15. The kinetic curves of the methyl-orange degradation in the presence of the $Mg_3Al_{0.5}Ti_{0.5}$-$T°C$-R_{H2O} samples and compared with commercial P25.
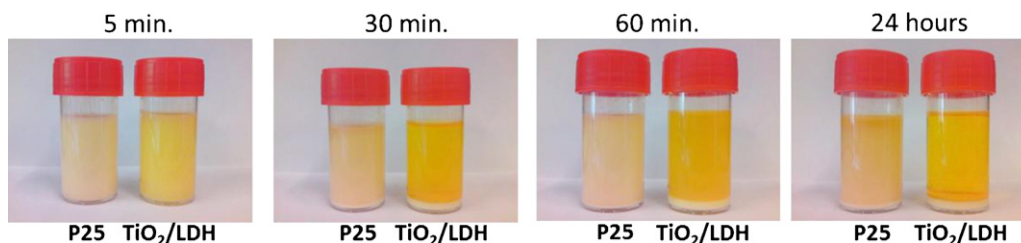

Fig. 16. Separation experiments.

groups, therefore the hydroxyl groups of brucite-like sheets may be less accessible, resulting in decreased photocatalytic efficiency, e.g. from 93% to 80%/h of reaction.

The low photocatalytic efficiency of the $Mg_3Al_{0.5}Ti_{0.5}$-$500°C$-R_{H2O} sample may be well correlated with the XRD and UV-vis DR observations which indicated that during the reconstruction process, almost all the Ti^{4+} cations are incorporated into the brucite-like sheets. Only minor traces of anatase phase could be detected on the surface of the brucite-like sheets leading to only 7% of dye removal after 1 h of reaction.

Comparing the photocatalytic activity of the $Mg_3Al_{0.5}Ti_{0.5}$-LDH with the photocatalytic activity of the commercial Degussa P25, it is clearly observed that the advantage of using such nanocomposites, combining TiO_2 with LDH-type structures, is that the process is improved by the decrease of the solid/liquid ratio as well as the decrease of the time for the removal of the dye (Fig. 15). Therefore, after 20 min of UV irradiation ∼90% of dye could be removed by the nanocomposites, showing a much stronger photo-oxidative effect than the commercial P-25 (∼15% efficiency after 20 min of UV irradiation).

Comparing the photocatalytic activity of the two types of nanocomposite systems, it may be concluded that the initial Ti^{4+} location has a direct influence on the quality and properties of the final products. The photocatalytic activity of the layered product in which the brucite-like sheets composition was altered prior to the reconstruction step was found to be higher than that of the nanocomposite system obtained by the reconstruction in $TiOSO_4 \cdot xH_2O$ aqueous solution. This may be due to the intimate contact created during the isomorphous substitution of the Ti^{4+} cations within the brucite-like network which facilitates the electron/hole transfer between the two phases increasing the efficiency of the charge separation, the entire system showing stronger

photocatalytic activity. Moreover, in the case of the TiO_2/Mg_3Al-LDH-1 h calcined at different temperatures, the results showed that structure in which the LDH phase is embedded into an anatase matrix are obtained, thus blocking structural OH groups of the LDH phase. Therefore, decreased photocatalytic efficiency was observed (89% for the sample calcined at 450 °C or 82% for the sample calcined at 750 °C) when comparing with the $Mg_3Al_{0.5}Ti_{0.5}$-LDH sample (93%).

Furthermore, catalyst recovering experiments were realized using the obtained nanocomposite samples in comparison to the commercial Degussa P25, which is well known as having difficulties in separation. It was observed that the obtained nanocomposites may be separated by natural sedimentation within minutes while P25 could not be separated in hours (Fig. 16).

4. Conclusions

We report the synthesis of some self-assembled nanocomposite systems based on TiO_2 and MgAl-LDHs structures. In order to study the influence of the initial Ti^{4+} location on the quality of the final products, different approaches were used by taking advantage of the memory effect property of the LDHs-type materials: first the structural reconstruction of a calcined MgAl-clay into a $TiOSO_4$ aqueous solution and, secondly, the structural reconstruction of a calcined MgAlTi-clay in water. It was demonstrated that different structural changes occur during the nanocomposite synthesis which are strongly related with the brucite-like sheets composition. It was found that the stage at which the Ti^{4+} cations were added has a direct influence on the quality and photocatalytic activity of the obtained nanocomposite systems. The ability of the obtained nanocomposites to degrade methyl-orange under UV-light was tested and compared with commercial Degussa P25.

An intimate contact has been created between the anatase and the brucite-like sheets in the nanocomposite systems, which had a direct influence on the HO• radical production enhancing thus the photocatalytic performances. $Mg_3Al_{0.5}Ti_{0.5}$-LDH sample manifests already very powerful photo-oxidative effect assigned to the segregation of small anatatse nanocrystals on the highly hydroxylated layered surface. Moreover, the photocatalytic activity could be tailored by controlling the thermal treatment of the obtained products. The advantages of using the TiO_2/LDHs nanocomposites for the photodegradation of MO dye in aqueous media are multiple, e.g. increased activity per mass, higher efficiencies at a decreased solid/liquid ratio, decreased reaction times, reduced agglomeration and easy to separate at the end of the processes.

Acknowledgements

References

[1] K.M. Parida, L. Mohapatra, Chemical Engineering Journal 179 (2012) 131–139.
[2] D. Chen, Y. Li, J. Zhang, J.-z. Zhou, Y. Guo, H. Liu, Chemical Engineering Journal 185–186 (2012) 120–126.
[3] A.V. Rupa, D. Manikandan, D. Divakar, T. Sivakumar, Journal of Hazardous Materials 147 (2007) 906–913.
[4] R. Comparelli, E. Fanizza, M.L. Curri, P.D. Cozzoli, G. Mascolo, A. Agostiano, Applied Catalysis B: Environmental 60 (2005) 1–11.
[5] G. Colón, J.M. Sánchez-España, M.C. Hidalgo, J.A. Navío, Journal of Photochemistry and Photobiology A: Chemistry 179 (2006) 20–27.
[6] S. Liao, H. Donggen, D. Yu, Y. Su, G. Yuan, Journal of Photochemistry and Photobiology A: Chemistry 168 (2004) 7–13.
[7] S.K. Kansal, M. Singh, D. Sud, Journal of Hazardous Materials 141 (2007) 581–590.
[8] E.M. Seftel, E. Popovici, E. Beyers, M. Mertens, H.Y. Zhu, E.F. Vansant, P. Cool, Journal of Nanoscience and Nanotechnology 10 (2010) 8227–8233.
[9] M. Shao, J. Han, M. Wei, D.G. Evans, X. Duan, Chemical Engineering Journal 168 (2011) 519–524.
[10] Z.P. Xu, P.S. Braterman, F. Yarberry, in: S.M. Auerbach, K.A. Carrado, P.K. Dutta (Eds.), Handbook of Layered Materials, Marcel Dekker Inc., New York, 2004, ISBN 9780824753498, p. 373.
[11] E.M. Seftel, E. Popovici, M. Mertens, K. Witte, G. Tendeloo, P. Cool, E.F. Vansant, Microporous and Mesoporous Materials 113 (2008) 296–304.
[12] F. Cavani, F. Trifirò, A. Vaccari, Catalysis Today 11 (1991) 173–301.
[13] A. Vaccari, Applied Clay Science 22 (2002) 75–76.
[14] G. Carja, A. Nakajima, S. Dranca, C. Dranca, K. Okada, The Journal of Physical Chemistry C 114 (2010) 14722–14728.
[15] G. Carja, A. Nakajima, C. Dranca, K. Okada, Journal of Nanoparticle Research 12 (2010) 3049–3056.
[16] G. Carja, Y. Kameshima, A. Nakajima, C. Dranca, K. Okada, International Journal of Antimicrobial Agents 34 (2009) 534–539.
[17] J. Olanrewaju, B.L. Newalkar, C. Mancino, S. Komarneni, Materials Letters 45 (2000) 307–310.
[18] R.L. Frost, A.W. Musumeci, T. Bostrom, M.O. Adebajo, M.L. Weier, W. Martens, Thermochimica Acta 429 (2005) 179–187.
[19] E.M. Seftel, E. Popovici, M. Mertens, G. Van Tendeloo, P. Cool, E.F. Vansant, Microporous and Mesoporous Materials 111 (2008) 12–17.
[20] E.M. Seftel, E. Popovici, M. Mertens, P. Cool, E.F. Vansant, Journal of Optoelectronics and Advanced Materials 10 (2008) 3477–3481.
[21] T. Lopez, E. Sanchez, P. Bosch, Y. Meas, R. Gomez, Materials Chemistry and Physics 32 (1992) 141–152.
[22] H.W. Olfs, L.O. Torres-Dorante, R. Eckelt, H. Kosslick, Applied Clay Science 43 (2009) 459–464.
[23] J.A. Rivera, G. Fetter, P. Bosch, Microporous and Mesoporous Materials 89 (2006) 306–314.
[24] J.A. Rivera, G. Fetter, Y. Jiménez, M.M. Xochipa, P. Bosch, Applied Catalysis A: General 316 (2007) 207–211.
[25] A.J. Marchi, C.R. Apesteguĭa, Applied Clay Science 13 (1998) 35–48.
[26] M. Intissar, F. Malherbe, V. Prévot, F. Leroux, Journal of Colloid and Interface Science 299 (2006) 747–753.
[27] S. Velu, K. Suzuki, T. Osaki, F. Ohashi, S. Tomura, Materials Research Bulletin 34 (1999) 1707–1717.
[28] J.T. Kloprogge, Clays and Clay Minerals 52 (2004) 795–797.
[29] I. Hannus, T. Tóth, D. Méhn, I. Kiricsi, Journal of Molecular Structure 563–564 (2001) 279–282.
[30] N. Das, A. Samal, Microporous and Mesoporous Materials 72 (2004) 219–225.
[31] S.P. Paredes, M.A. Valenzuela, G. Fetter, S.O. Flores, Journal of Physics and Chemistry of Solids 72 (2011) 914–919.
[32] K. Lv, J. Yu, K. Deng, X. Li, M. Li, Journal of Physics and Chemistry of Solids 71 (2010) 519–522.